Hindawi
Journal of Advanced Transportation
Volume 2018, Article ID 6986198, 19 pages
https://doi.org/10.1155/2018/6986198

Research Article

Vertical and Horizontal Queue Models for Oversaturated Signal Intersections with Quasi-Real-Time Reconstruction of Deterministic and Shockwave Queueing Profiles Using Limited Mobile Sensing Data

Yongyang Liu,[1] Jingqiu Guo,[2] and Yibing Wang[1]

[1] *Institute of Intelligent Transportation Systems, Zhejiang University, 866 Yuhangtang Road, Hangzhou 310058, China*
[2] *College of Transportation Engineering, Key Laboratory of Road and Traffic Engineering of the Ministry of Education, Tongji University, 201804, China*

Correspondence should be addressed to Yibing Wang; wangyibing@zju.edu.cn

Received 16 August 2017; Revised 3 January 2018; Accepted 18 January 2018; Published 10 June 2018

Academic Editor: Andy Chow

Deterministic/point/vertical and shockwave/physical/horizontal queueing models are widely used in traffic operation to estimate vehicular queue length and delays at bottlenecks such as signalized intersections. The consistency between the two types of queueing model in terms of their estimation performance has been a subject of debate for decades. This paper reexamines the issue, typically with respect to oversaturated signal intersections, and demonstrates the consistency based on analytical studies and microscopic simulations. While fixed-location sensor data was dominating, it was hardly possible to construct the deterministic or shockwave queueing profile using real data. For this reason, either profile had significance only at a conceptual level and could not be put into practical usage. With the quick spread of mobile sensing data, however, the situation has drastically changed. In this context, this paper also intends to develop an efficient approach to the reconstruction of the deterministic and shockwave queueing profiles in a quasi-real-time manner using very limited mobile sensing data. Microscopic simulations with AIMSUN have demonstrated the efficiency of the approach as well as the analytical results obtained in this paper.

1. Introduction

This paper studies the consistency of the vertical and horizontal queue models as well as the quasi-real-time reconstruction of the deterministic and shockwave queueing profiles using very limited mobile sensing data for oversaturated signal intersections.

The vertical and horizontal queue models are two distinctive queueing models widely used in transport and traffic engineering. The vertical queue model provides a physically impossible but conceptually valid description of queueing processes. It postulates that any vehicle that has to queue before passing a bottleneck is stacked in a vertical pile at the bottleneck, on top of any other such vehicles that arrived earlier. When the queue is released, departing vehicles exit from the bottom of the queue. A vertical queue does not occupy any road space and has no influence on upstream approaching vehicles. It is therefore also called a point queue. In contrast, the horizontal queue model formulates the formation and dissipation of a physical queue. Figure 1 illustrates the two types of queue with respect to a signalized intersection.

The deterministic queueing profile is commonly used to describe the vertical queueing process. It is based on cumulative diagrams, which were initially introduced to transport by Moskowitz and Newman [1] and Gazis and Potts [2] and later highlighted by Newell for the potential as a traffic analysis tool (Daganzo [3]). On the other hand, the shockwave queueing profile is based on traffic flow theory [4, 5] to describe the spatiotemporal dynamics of the horizontal queues. Both queueing profiles are depicted in Figure 2 for an oversaturated signal intersection.

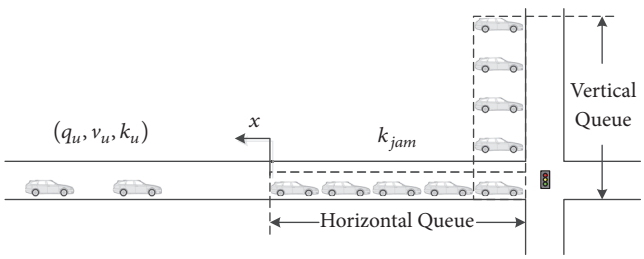

Figure 1: The horizontal and vertical queue models for a signalized intersection (x and k_{jam} are given in Figure 5).

The consistency of the vertical and horizontal queue models or equivalently of the deterministic and shockwave queueing profiles (in terms of their modeling performance) is of much interest and has been a subject of debate for decades. Several textbooks and handbooks have described the two models or two queueing analysis methods as separate tools for treating bottleneck problems (see, e.g., McShane and Roess [6]). Makigami et al. [7] studied the two analysis methods using a three-dimensional (space-time-queue) model and demonstrated their consistency. Wirasinghe [8] proved that the two methods delivered identical results in the total travel delay. Michalopoulos and Pisharody [9] however commented that the deterministic profile overestimated travel delays, while Daganzo [10] pointed out a flaw in that work and emphasized that, with the flaw removed, the two methods were still consistent. More than a decade later, the inconsistency issue was again raised by Chin [11], McShane and Roess [6], and Nam and Drew [12], whereas Lawson et al. [13], Erera et al. [14], Daganzo [3], and Lovell and Windover [15] underlined the consistency once more. More recently, Rakha and Zhang [16] and Yi et al. [17] concurred with the consistency but tried to improve Nam and Drew's approach [12].

The vertical and horizontal queue models are quite different in their operational mechanisms, which is very much the reason for the consistency issue to be raised from time to time. With the literature review, we see that thorough and analytical investigations on the issue still lack. This paper intends to close the debates via a systematic study, particularly for the case of oversaturated signal intersections. This is actually the first motivation of the current work.

Traffic signals are one of the crucial components of traffic networks. Queue length [8, 18–20] and total delay [6, 8, 20, 21] of vehicles due to signal operation are among the most important performance measures for traffic signal control. Many relevant studies were conducted using the deterministic queueing profile [8, 10, 12, 15, 20] or shockwave queueing profile [8, 18, 19] with fixed-location sensing data (e.g., loop detector data). As a matter of fact, both deterministic and shockwave queueing profiles are individual-vehicle-trajectory oriented. Fixed-location sensors can hardly provide sufficient information for constructing either profile for the purpose of traffic signal control. For this reason, while fixed-location sensing technologies were dominating, both queueing profiles only had significance at a conceptual level and could not offer strong operability in practice. In recent years, however, the emergence of mobile sensing technologies based on connected vehicles (CVs) has been attracting increasingly more attention. Equipped with GPS (or other tracking devices) and wireless communication systems, CVs are able to provide real-time information (of their positions, speeds, and acceleration), thus leading in total to better spatial coverage of traffic conditions. This has also offered opportunities of reexamining the two queueing models/profiles for traffic modeling and signal control.

A number of studies have been conducted using mobile sensing data, to address shockwave profile reconstruction for the purpose of queue length estimation [22–26]. The focus of those works is on the identification of some critical points on vehicle trajectories based on the shockwave model. For instance, [22] tried to figure out the critical points that fall on the congestion forming shockwave curves (CFSC) to determine vehicle trajectories. The work in [24] fitted vehicle trajectories with piecewise linear lines and took critical points as the intersection of the lines. The work in [25] fixed the critical points using both speed and acceleration information. The work in [26] formulated the construction of CFSC as a convex optimization problem. In addition, [27–29] studied queueing delay patterns using mobile-sensing-based travel time data and estimated queue length for signalized intersections. So far, still missing is a simple and efficient approach to the reconstruction of shockwave queueing profiles using mobile sensing data, and this is the second motivation of the current work.

It should be noted that only the shockwave queueing profiles can be directly reconstructed using mobile sensing data. Due to its abstract nature, the deterministic queueing profile can only be built upon the corresponding shockwave queueing profile in consideration of the consistency between the two profiles.

To sum up, the objective of this work is twofold. First, it aims to close the debates on the consistency of the two queueing models via some systematic and analytical studies. Second, it intends to develop an efficient approach to the reconstruction of the shockwave and deterministic queueing profiles in a quasi-real-time manner using very limited mobile sensing data. The work was done with regard to oversaturated signal intersections. Microscopic simulation tool AIMSUN was used to deliver emulated mobile sensing data and evaluate the accuracy of queueing profile reconstruction, with various penetration rates of connected vehicles taken into account.

The remainder of the paper is organized as follows. Section 2 introduces the vertical and horizontal queue models as well as the deterministic and shockwave queueing profiles with respect to an oversaturated signal intersection. The consistency properties of the two queueing models/profiles are presented in Section 3. Section 4 focuses on the quasi-real-time reconstruction of the two queueing profiles using very limited mobile sensing data. Section 5 reports on simulation studies, with satisfactory results delivered. Section 6 concludes the paper.

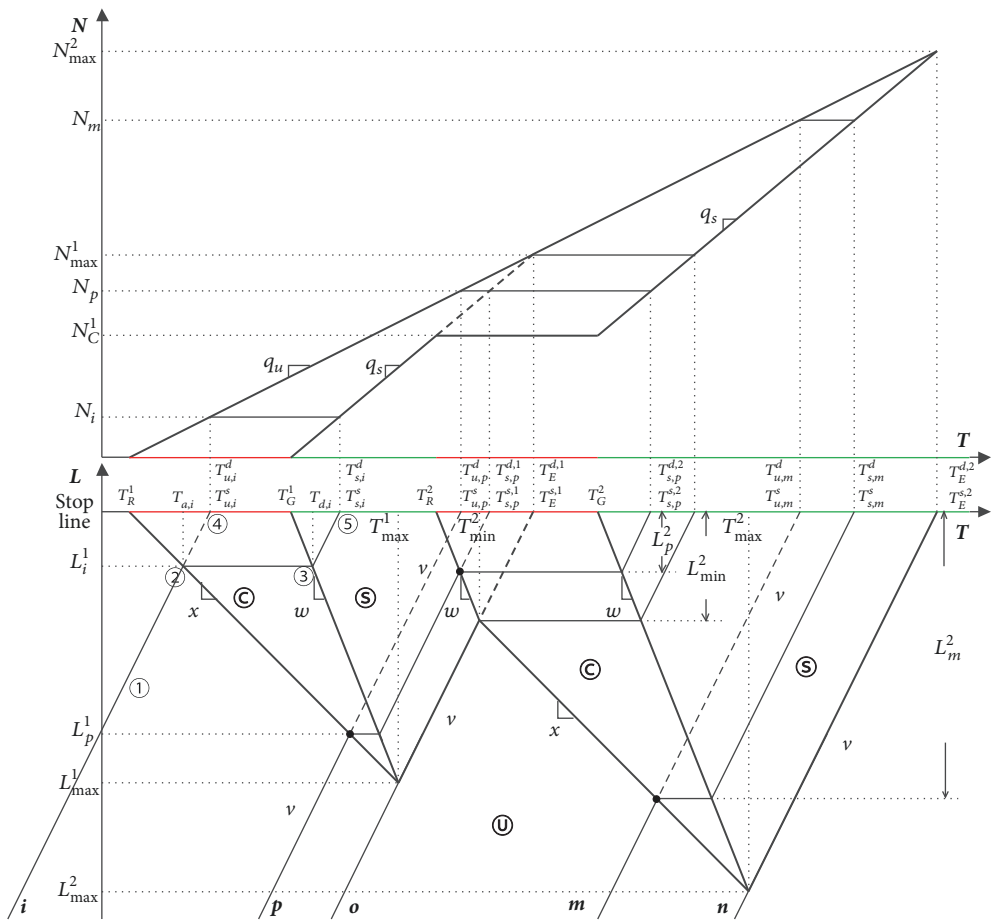

Figure 2: Deterministic and shockwave queueing profiles for an oversaturated signal intersection (traffic conditions ⓒ, ⓢ, and ⓤ are defined with Figure 5).

2. Queueing Models for Oversaturated Signal Intersections

2.1. Vertical and Horizontal Queue Models. With reference to Figure 1, either queueing model takes as an input-output system the displayed road link between the upstream entry and the downstream intersection. Consider one vehicle and its counterpart enter the road link at the same time and experience the horizontal and vertical queueing, separately. The two vehicles should pass the stop line at the intersection at the same time. This is actually a minimum requirement for the two queueing models; i.e., given the same input, the model outputs should be the same, despite quite different internal mechanism of queueing.

The two queueing models can be further examined with Figures 3 and 4. Figure 3 depicts a queue forming process over a red signal phase at the intersection and focuses on three typical time instants: (a) both vertical and horizontal queues exist with three vehicles A, B, and C, while D is approaching either queue; (b) D just joins the horizontal queue while it is still running towards the vertical queue at the stop line; (c) D reaches the stop line and becomes the new tail of the vertical queue. Focusing on vehicle D, we see

(i) it makes no difference to the two types of queue before time instant (b);

(ii) it joins the horizontal queue earlier than the vertical queue;

(iii) after joining the horizontal queue it keeps its original speed until joining the vertical queue;

(iv) the process with which it joins the vertical queue as depicted in Figure 2(c) is completed instantaneously.

Figure 4 displays a queue dissolving process and focuses on three typical time instants: (a) vehicles are queueing right before the end of a red signal phase; (b) vehicles A and B have already passed the stop line, and vehicle C is waiting in the vertical queue at the stop line while it has departed from the horizontal queue and is running towards the stop line; (c) vehicle C is passing the stop line from both queues. The process that C departs from the vertical queue to pass the stop line is completed instantaneously. In summary,

(i) a horizontal queue makes a distinction between "departing from the queue" and "passing the stop line", while a vertical queue does not;

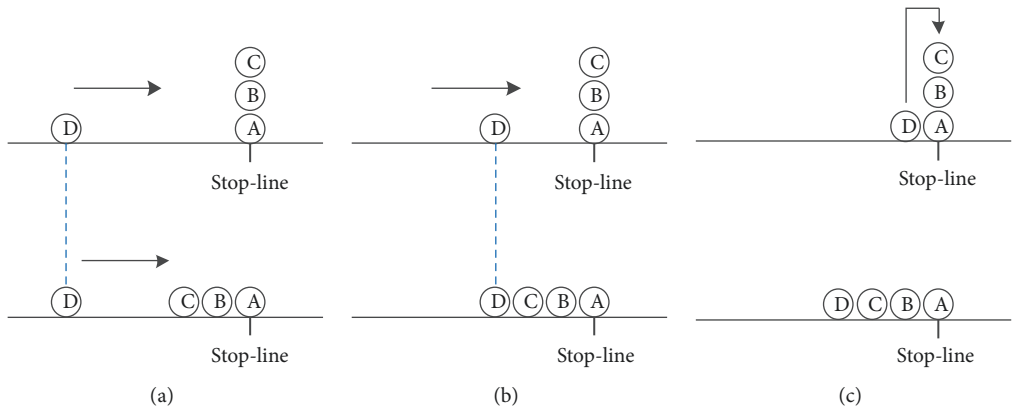

Figure 3: Vehicles arrive to join a vertical queue (upper) and a horizontal queue (lower) over a red signal phase: (a) when D is approaching either queue; (b) when D just joins the horizontal queue; (c) when D just joins the vertical queue.

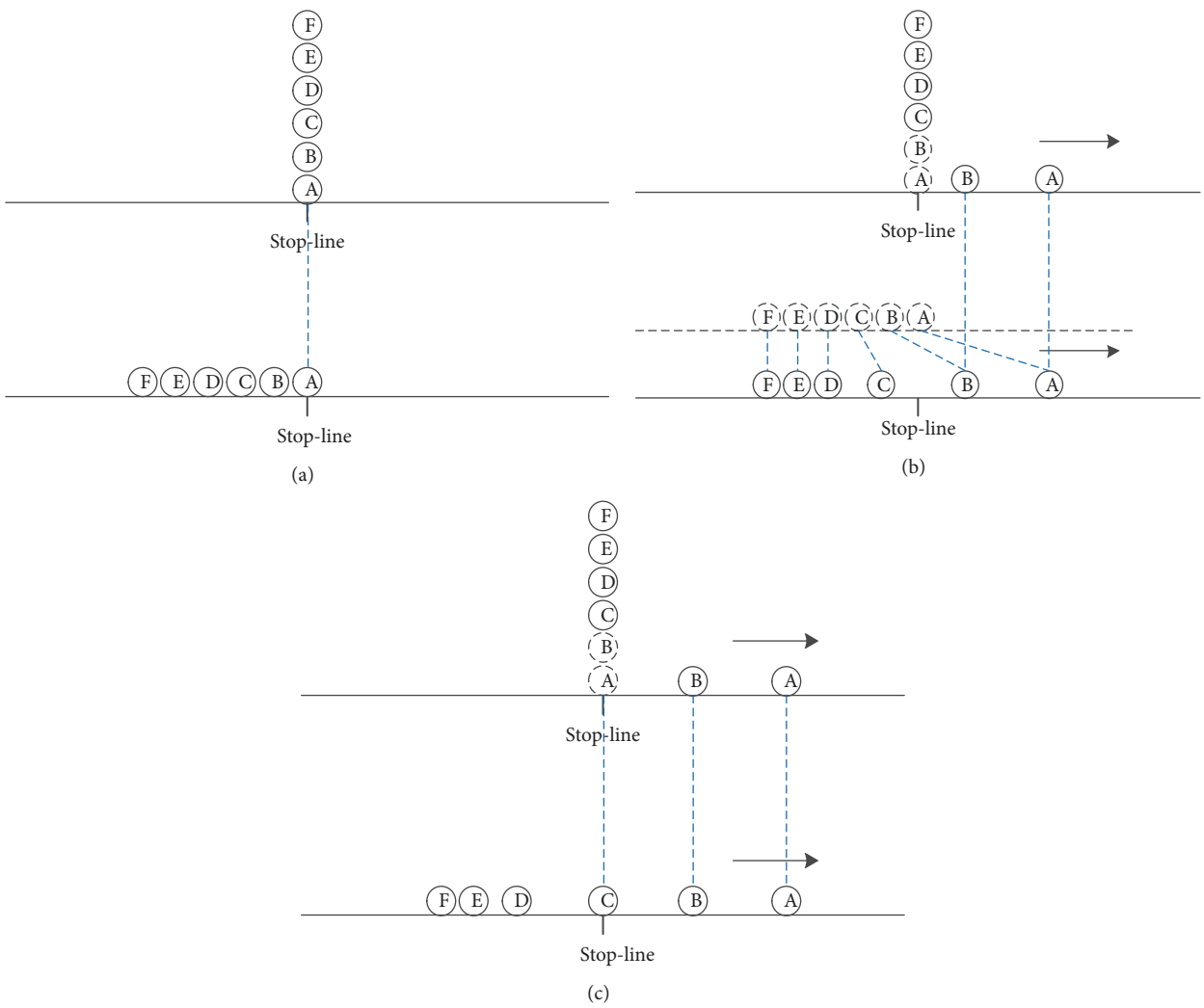

Figure 4: Vehicles depart from a vertical queue (upper) and a horizontal queue (lower): (a) vehicles are all queueing before the end of a red phase; (b) C has departed from the horizontal queue but is still waiting in the vertical queue; (c) C is passing the stop line from both queues.

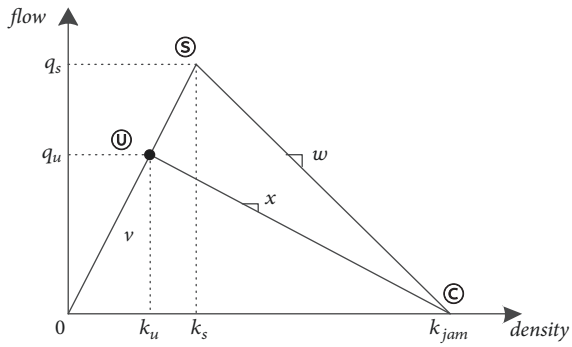

Figure 5: A triangular fundamental diagram.

(ii) a horizontal queue vehicle and its counterpart in the vertical queue pass the stop line at the same time.

2.2. Deterministic and Shockwave Queueing Profiles. With reference to Figure 1, traffic conditions along the road link and at the intersection are defined with the fundamental diagram in Figure 5. More specifically $U(q_u, k_u, v)$, $S(q_s, k_s, v)$, and $C(0, k_{\text{jam}}, 0)$ address the upstream arrival flow, the capacity flow at the intersection, and the queueing condition on the road link, with x and w denoting the queue forming and dissolving shockwaves.

Without loss of generality, Figure 2 plots the deterministic and shockwave queueing profiles for the intersection under signal oversaturation over two cycles. A number of definitions and notations are first given. On the time axes, T_R^1, T_G^1, T_R^2, and T_G^2 represent the start and end times of red phases. The superscripts "d" and "s" of symbols on the time axes refer to the "deterministic" and "shockwave" queueing profiles, respectively. The two profiles are connected via individual vehicle trajectories; see, e.g., vehicles i, p, and m. As a consequence, a number of time instants appear in pairs, e.g., $T_E^{d,1} = T_E^{s,1}$, $T_E^{d,2} = T_E^{s,2}$, $T_{u,\varphi}^d = T_{u,\varphi}^s$, $T_{s,\varphi}^d = T_{s,\varphi}^s$ ($\varphi = i, p, m$). $T_E^{d,2}$ (or $T_E^{s,2}$) denotes the time instant by which vehicles that are delayed over the two cycles have all been served, while $T_E^{d,1}$ (or $T_E^{s,1}$) is a virtual time instant by which all vehicles delayed over the first cycle would have been served without signal oversaturation. $T_{u,\varphi}^d$ or $T_{u,\varphi}^s$ denotes the time vehicle φ joins the vertical queue, and $T_{s,\varphi}^d$ or $T_{s,\varphi}^s$ denotes the time vehicle φ leaves the vertical queue (or equivalently passes the stop line with both queues). The timewise consistency between the two profiles is discussed later with Theorems 1 and 2. Moreover, $T_{\max}^1$ and $T_{\max}^2$, defined only for the shockwave profile, are the time instants the physical queues spill back to reach their far ends.

On the N axis of the deterministic profile, N_C^1 refers to the actual number of vehicles served by the end of the first cycle, $N_{\max}^2$, corresponding to $T_E^{d,2}$ (or $T_E^{s,2}$), refers to the total number of vehicles that are delayed but eventually served over the two cycles, and $N_{\max}^1$, corresponding to $T_E^{d,1}$ (or $T_E^{s,1}$), is a virtual quantity addressing the number of vehicles that would have been served by the end of the first cycle without signal oversaturation. In addition, N_i, N_p, and N_m denote the accumulative numbers for vehicles i, p, and m in the vertical queue.

On the L axis of the shockwave profile, L_φ^θ denotes the distance between vehicle φ and the stop line when it joins the horizontal queue in cycle θ. $L_{\max}^1$ and $L_{\max}^2$, corresponding to $T_{\max}^1$ and $T_{\max}^2$, respectively, address the far ends that the physical queues can reach.

In the case of signal oversaturation over two cycles, some vehicles are involved with the horizontal queue once, while some others may experience queueing twice. With "single" queueing, a vehicle φ joins and leaves the vertical queue at $T_{u,\varphi}^d$ and $T_{s,\varphi}^d$ (e.g., vehicles i and m). With "double" queueing, a vehicle φ (e.g., vehicle p) joins the vertical queue at $T_{u,\varphi}^d$ and would leave it at $T_{s,\varphi}^{d,1}$ if there was no oversaturation but factually leaves it at $T_{s,\varphi}^{d,2}$. Accordingly, the timewise consistency between the two profiles reads $T_{u,\varphi}^d = T_{u,\varphi}^s$; $T_{s,\varphi}^d = T_{s,\varphi}^s$ or $T_{s,\varphi}^{d,1} = T_{s,\varphi}^{s,1}$ and $T_{s,\varphi}^{d,2} = T_{s,\varphi}^{s,2}$.

When a vehicle φ joins a horizontal queue, its distance from the stop line follows a different way of definition. If φ joins the horizontal queue only in cycle 1, then only L_φ^1 is defined (e.g., $\varphi = i$); if it joins the queue only in cycle 2, only L_φ^2 is defined (e.g., $\varphi = m$); if it joins the queue twice, both L_φ^1 and L_φ^2 (e.g., $\varphi = p$) make sense.

3. Consistency Properties of the Queueing Profiles

The consistency properties of the two queueing profiles are described via four theorems and one corollary. The mathematical proof is found in Appendices A and B. To the best of our knowledge, these properties were not explicitly discussed, especially for oversaturated signal intersections. The theorems and corollary are presented on the basis of Figure 2, with respect to signal oversaturation over two cycles, but also apply to more general cases.

Theorem 1. *For a signal cycle θ ($\theta = 1, 2$), $T_E^{s,\theta} = T_E^{d,\theta}$.*

Proof. See Appendix A. □

With reference to Figure 2, $T_E^{s,1}$ and $T_E^{d,1}$ are two virtual quantities while $T_E^{s,2}$ and $T_E^{d,2}$ are well defined. The theorem says that the two types of queue are cleared at the same time in the case of either undersaturation ($\theta = 1$) or oversaturation ($\theta = 2$).

Theorem 1 sets a basis for the proof of the other theorems and corollary. Following Theorem 1, $T_E^{d,\theta}$ and $T_E^{s,\theta}$ ($\theta = 1, 2$) are replaced with T_E^θ ($\theta = 1, 2$) in the sequel.

Theorem 2. *Consider a vehicle φ and its counterpart, which go through the vertical and horizontal queues separately. Then,*

(1) the vehicles do not join the two queues at the same time, but $T_{u,\varphi}^s = T_{u,\varphi}^d$;

(2) the vehicles do not depart from the queues at the same time but pass the stop line at the same time, i.e., $T^{s}_{s,\varphi} = T^{d}_{s,\varphi}$ *or* $T^{s,\theta}_{s,\varphi} = T^{d,\theta}_{s,\varphi}$ $(\theta = 1, 2)$.

Proof. See Appendix A. □

Regarding the property demonstrated with Theorem 2-(2), see also Section 2.1.

Corollary 3. *Given a vehicle* φ*, its total horizontal queue delay* d^{s}_{φ} *is equal to its vertical queue delay* d^{d}_{φ}.

Proof. See Appendix A. □

This may also be checked graphically with, e.g., vehicle i in Figure 2. The trajectory of vehicle i in the shockwave profile is ②③⑤, while ②④⑤ is its vertical queue trajectory in time. Clearly, vehicle i spends the same period of time in both profiles, i.e., between ④ and ⑤ for the vertical queue and between ② and ③ for the horizontal queue.

Theorem 4. *For any vehicle* φ *in a signal cycle* θ $(\theta = 1, 2)$,

$$\begin{gathered} N_{\varphi} - N^{\theta-1}_{C} = L^{\theta}_{\varphi} \cdot k_{\text{jam}} \\ T^{\theta}_{G} \le T^{s,\theta}_{s,\varphi} \le T^{\theta}_{E}, \end{gathered} \tag{1}$$

where $N^{0}_{C} = 0$, $N^{1}_{C} = q_s \cdot (T^{2}_{R} - T^{1}_{G})$.

Proof. See Appendix A. □

Any vehicle φ and its counterpart do not join the horizontal queue and the corresponding vertical queue at the same time, but their positions in the queues (N_{φ} and L^{θ}_{φ}) are interrelated as stated above. With reference to Figure 2, only L^{1}_{i} is defined for vehicle i; then $N_i = L^{1}_{i} \cdot k_{\text{jam}}$; both L^{1}_{p} and L^{2}_{p} are defined for vehicle p; then $N_p = L^{1}_{p} \cdot k_{\text{jam}}$ and $N_p - N^{1}_{C} = L^{2}_{p} \cdot k_{\text{jam}}$; only L^{2}_{m} is defined for vehicle m; then $N_m - N^{1}_{C} = L^{2}_{m} \cdot k_{\text{jam}}$.

It is noted that Theorem 4 also applies to more general cases with $\theta > 2$, where $N^{\theta}_{C} = q_s \cdot (T^{\theta+1}_{R} - T^{\theta}_{G})$. The proof is omitted.

Corollary 5. *For any vehicle* φ *that experiences queueing more than once,*

$$L^{2}_{\varphi} = L^{1}_{\varphi} - \frac{\left(T^{2}_{R} - T^{1}_{G}\right) \cdot q_s}{k_{jam}} \tag{2}$$

Proof. See Appendix A. □

Given a vehicle φ that experiences queueing more than once over multiple signal cycles, the corollary formulates the relation of this vehicle's queue length in two neighboring cycles.

It is noted that Corollary 5 also applies to more general cases with $\theta > 2$:

$$L^{\theta+N}_{\varphi} = L^{\theta}_{\varphi} - \frac{\sum_{i=1}^{N}\left(T^{\theta+i}_{R} - T^{\theta+i-1}_{G}\right) \cdot q_s}{k_{\text{jam}}} \tag{3}$$

The proof is omitted.

Theorem 6. *The total delays created by the vertical and horizontal queueing models are equal, i.e.,* $S_V = S_H \cdot k_{jam}$*, where* S_V *is the total area of the deterministic queueing profile over the whole period* $[T^{1}_{R}, T^{d,2}_{E}]$ *in Figure 2, while* S_H *is the total area of the two shockwave polygons over periods* $[T^{1}_{R}, T^{1}_{max}]$ *and* $[T^{2}_{R}, T^{2}_{max}]$ *in Figure 2.*

Proof. See Appendix A. □

So far what has been discussed with Figure 2 is the case of a constant traffic demand. The theorems and corollary can certainly be extended to the case of a varying traffic demand (Figure 6), and the corresponding proof is found in Appendix B.

4. Quasi-Real-Time Reconstruction of Queueing Profiles Using Limited Mobile Sensing Data

Conventional fixed-location detectors such as loops, radars, and cameras cannot provide sufficient or suitable measurements to construct the deterministic and shockwave queueing profiles. Albeit well-known in traffic engineering, the vertical/horizontal queue models and the deterministic/shockwave queueing profiles have long been considered only at a conceptual level. With the emergence of the mobile sensing technologies, however, the increasingly wider spread of mobile sensing data has made it possible to construct both queueing profiles in quasi-real time. In fact, what can be directly created using mobile sensing data is the shockwave queueing profile, but with the consistency properties presented in Section 3, especially Theorems 1, 2, and 4, the deterministic profile can also be constructed. As an illustrative example, Figure 7(a) presents the shockwave profiles constructed using mobile sensing data emulated with the microscopic simulation tool AIMSUN. The shockwave profiles over the five most congested cycles are highlighted, over which the corresponding signal intersection is oversaturated. Figure 7(b) displays the associated deterministic profile. The approaches employed to create both profiles are described in this section, and more simulation details are found in Section 5.

4.1. Basic Ideas. Given an intersection as shown in Figure 8, its arriving flow may consist of several components, according to the signal phase setting at the intersection right upstream: the through movement in phase (a); the right-turn movement during phase (c); the left-turn movement within phase (d). As an illustrative example, Figure 7(a) presents the correspondence of flows reaching the downstream intersection to the upstream signal phases as given in Figure 8.

Based on vehicle to vehicle/infrastructure communication, assume with reference to Figure 8 that the start and end times of each signal phase of the two intersections are known, and each movement towards the downstream intersection as shown in Figure 8 (i.e., each flow in Figure 7(a)) contains at least two connected vehicles (CVs). Then, each linear section of the congestion forming shockwave curve (CFSC) as shown

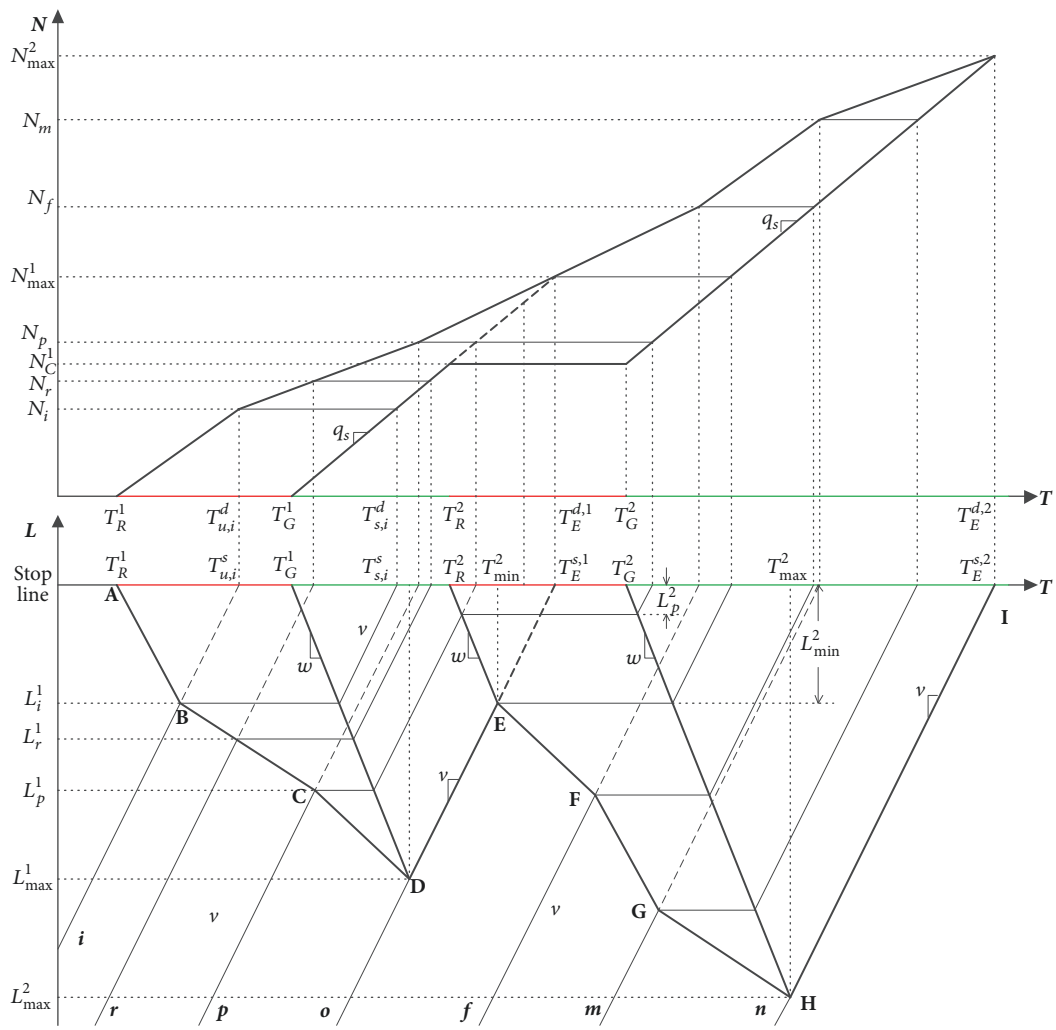

Figure 6: Deterministic and shockwave profiles under varying traffic demands.

in Figure 9 contains at least two measured points (e.g., y_0 and y_1), and the whole CFSC can be basically determined in quasi-real time. Similarly, the congestion dissolving shockwave w can also be determined. w is supposed to be constant by Figure 5, which is also confirmed with Figure 7(a) in simulation. Clearly, the more the CVs are available, the more accurately the shockwave profile is identified. This way of determining the shockwave profile was also considered in [12, 13, 15] via linear optimization. Once the shockwave profile is fixed, the deterministic profile can be readily determined as well.

Consider a CV i in Figure 9. The information of its positions and speeds as well as the corresponding time instants is available along its trajectory, e.g., at points y_1, y_3, and y_4. By Theorem 2 and the definition of the vertical queue, the time it joins the deterministic queueing profile at y_5 is equal to the time instant it reaches virtually y_2. y_2 can be approximately determined as $(1/n) \cdot \sum_{k=1}^{n} [t_k + L(t_k)/v(t_k)]$, where n denotes a given number of data points collected right before it joins the horizontal queue at y_1, $L(t_k)$ denotes its distance from the stop line at each time instant t_k, and $v(t_k)$ denotes the instantaneous speed. By Theorem 2, y_6 and y_4 are consistent in time. Moreover, based on Theorem 4, it is straightforward to get N_i for the deterministic profile with measured L_i in the shockwave profile. Thus, the full coordinates of y_5 and y_6 are fixed. As such, as long as two CVs are available for each portion of the arrival flow, both shockwave and deterministic queueing profiles can basically be determined; see, e.g., Figure 9.

4.2. Creating a Shockwave Profile

4.2.1. The Case of Two Connected Vehicles in Each Subflow. As previously mentioned, traffic arriving at an intersection can be decomposed into several flow portions as regulated by the signal phases at the intersection right upstream. There may also be a number of periods over which no vehicle arrives at the intersection. Such periods may appear in the middle of a CFSC, e.g., between flows ① and ② in Figure 7(a), or at the end of a CFSC, e.g., between flows ② and ③ in

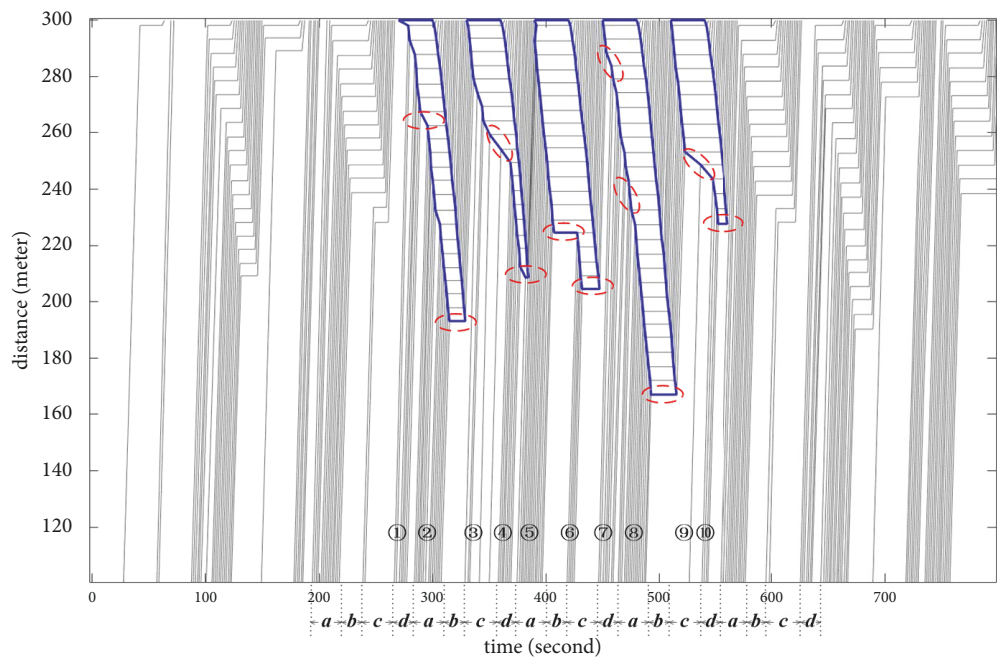

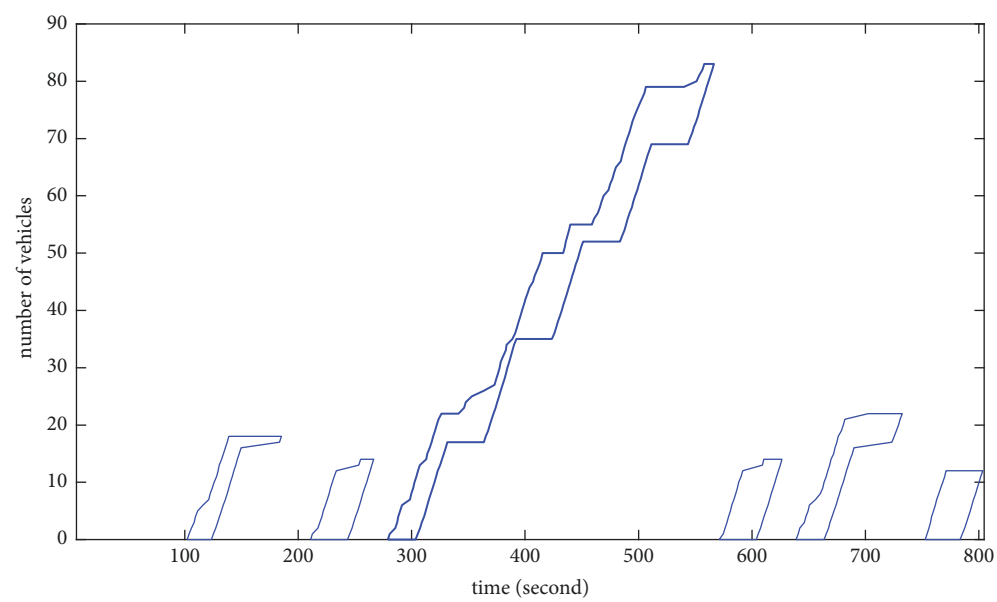

Figure 7: Queueing profiles based on microscopic simulation with 100% penetration rate of CVs: (a) shockwave profile (with the signal phases at the upstream intersection); (b) the corresponding deterministic profile.

Figure 7(a). Note that there are two possibilities concerning no vehicle arrival at a subject intersection: (1) the signal phase of the upstream intersection is prohibitive (e.g., phase (b) in Figure 8 and Figure 7(a)); (2) the upstream signal phase is permissive but by coincidence there is no demand; see in Figure 7(a), e.g., phase (d) in relation to flow ① and phase (c) to flow ⑥. Either case may occur in the middle of or at the end of a CFSC. It is stipulated in this work that if no vehicle arrival happens in the middle of a CFSC, the portion of CFSC concerning (1) is plotted as a horizontal line, e.g., between flows ⑤ and ⑥ in Figure 7(a), and the portion concerning (2) is plotted as a line, e.g., between ① and ② in Figure 7(a). However, if either (1) or (2) happens at the end of a CFSC, the corresponding portion is naturally plotted as a horizontal line, e.g., between ② and ③ and between ⑥ and ⑦ in Figure 7(a).

It is noted that Figure 7(a) plots the case of 100% penetration rate of CVs, where every trajectory displayed corresponds to one specific CV. However, the market penetration rate of CVs will be low in the foreseeable future, which means,

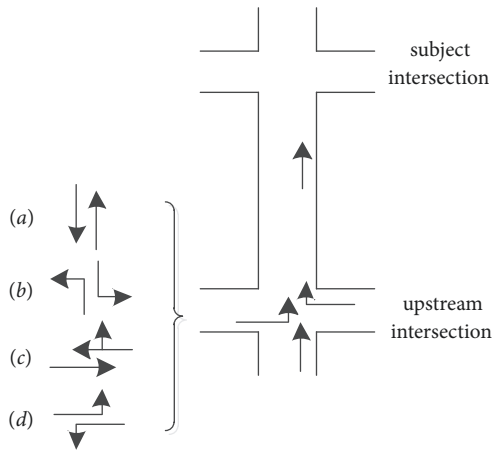

Figure 8: Arrival flow from upstream intersection.

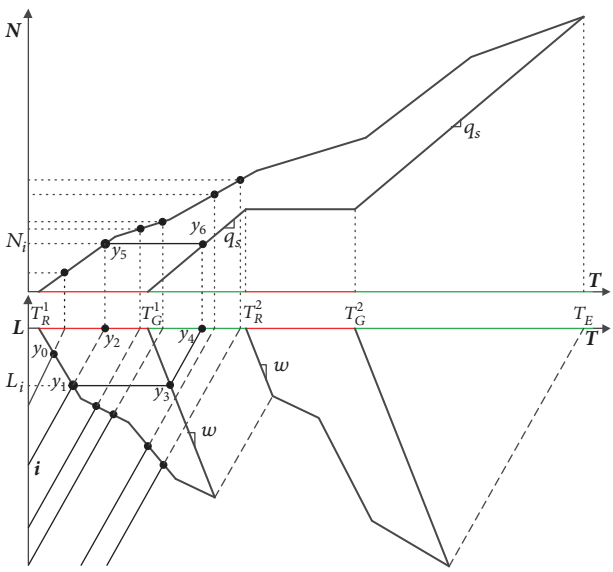

Figure 9: Two queueing profiles with variant upstream arrival flow.

in the context of Figure 7(a), only a very small number of vehicle trajectories displayed are actually observable. It is then a question how to construct the shockwave profile and accordingly the deterministic profile using very limited vehicle trajectory data. To be realistic, we assume in this work that each flow as shown in Figure 7(a) contains at most two CVs.

While constructing the shockwave profile using very limited mobile sensing data, it is common to encounter the situation of missing data. Six possible cases are presented in Figure 10. Figures 10(a) and 10(b) address the occurrence of missing data in the middle of CFSCs, while Figures 10(c)–10(f) address the cases at the end of CFSCs. Note that on top of "low penetration of CVs", "no vehicle arrival" as previously discussed also contributes to the result of missing data.

In Figure 10, CVs r and s correspond to one green phase of the upstream intersection, while CVs e and f correspond to the next green phase. Each of subfigures (b), (d), and (f) involves a prohibitive phase (e.g., phase (b) in Figure 8 and period OD in Figure 10(b)), while none of subfigures (a), (c), and (e) involves such a phase. Moreover, m represents a virtual vehicle that leaves the upstream intersection at the start of the next green phase, and virtual vehicle n leaves at the end time of the current green phase, which is followed by a prohibitive phase. Taking Figure 7(a) as the ground truth (with the 100% market penetration), all cases in Figure 10 except (e) and (f) are encountered while estimating both profiles using very limited mobile sensing data as sampled from Figure 7(a). More details are given in Section 5.

In what follows, we discuss how to treat the cases shown in Figure 10, with various situations of missing data taken into account, so as to reconstruct the shockwave profiles. In Figure 10(a), CVs r and s are from one green phase of the upstream intersection while CVs e and f correspond to another. It is not difficult to distinguish this since the information of all signal phases and of CVs are available. As such, y_2 is related to the last CV of that green phase, and y_3 is to the first CV of the next green phase. Then, two linear portions of CFSC can be determined, respectively, with CV data points y_1, y_2, y_3, and y_4. Note that the start time of the upstream green phase for e and f is known. Let a virtual vehicle m leave the upstream intersection at this time instant; the trajectory of m can be drawn with its slope equal to the mean speed of e and f. As such, points D and C can be fixed. It is noted that the portion of the congestion forming shockwave curve (CFSC) between y_1 and D belongs to the previous green phase. As such, there exist two extreme but possible cases: (1) y_2CD, i.e., section y_1C is with a constant traffic volume while no vehicle arrives over period CD; (2) y_2D, i.e., sections y_1y_2 and y_2D are with different traffic volumes. Moreover, between cases (1) and (2), there are a number of intermediate possibilities as displayed. Note that the ground truth can be any of the above cases. Based on our simulation results in Section 5, we believe case y_2D is more likely to happen than y_2CD.

Figure 10(b) refers to the case that a no-flow phase OD is involved. In this case, let virtual vehicle n leave the upstream intersection at the end time of the green phase associated with vehicles r and s; then the trajectory of n is fixed with its speed equal to the mean speed of vehicles r and s. As such, point O can be determined. The treatment of the portion between y_2 and O in Figure 10(b) is the same as that between y_2 and D in Figure 10(a).

Figures 10(c)–10(f) address the case that the data is missing at the end of a CFSC. First, we consider Figure 10(c), where CVs e and f from the next green phase of the upstream intersection do not join the queue in the cycle of the subject intersection for vehicles r and s, and this is also assumed to be the case for all vehicles from the next green phase (among them only e and f are observable). Let virtual vehicle m leave the upstream intersection at the start of the next green phase, and then points C and D can be fixed with the information of y_1, y_2, y_3, and y_4. Figure 10(d) refers to a similar case but the signal phase next to that for CVs r and s is a prohibitive phase. Let virtual vehicle n leave the upstream intersection at the end of the current green phase, and points C and D can be fixed. Note that CD in Figure 10(c) or 11(d) represents an

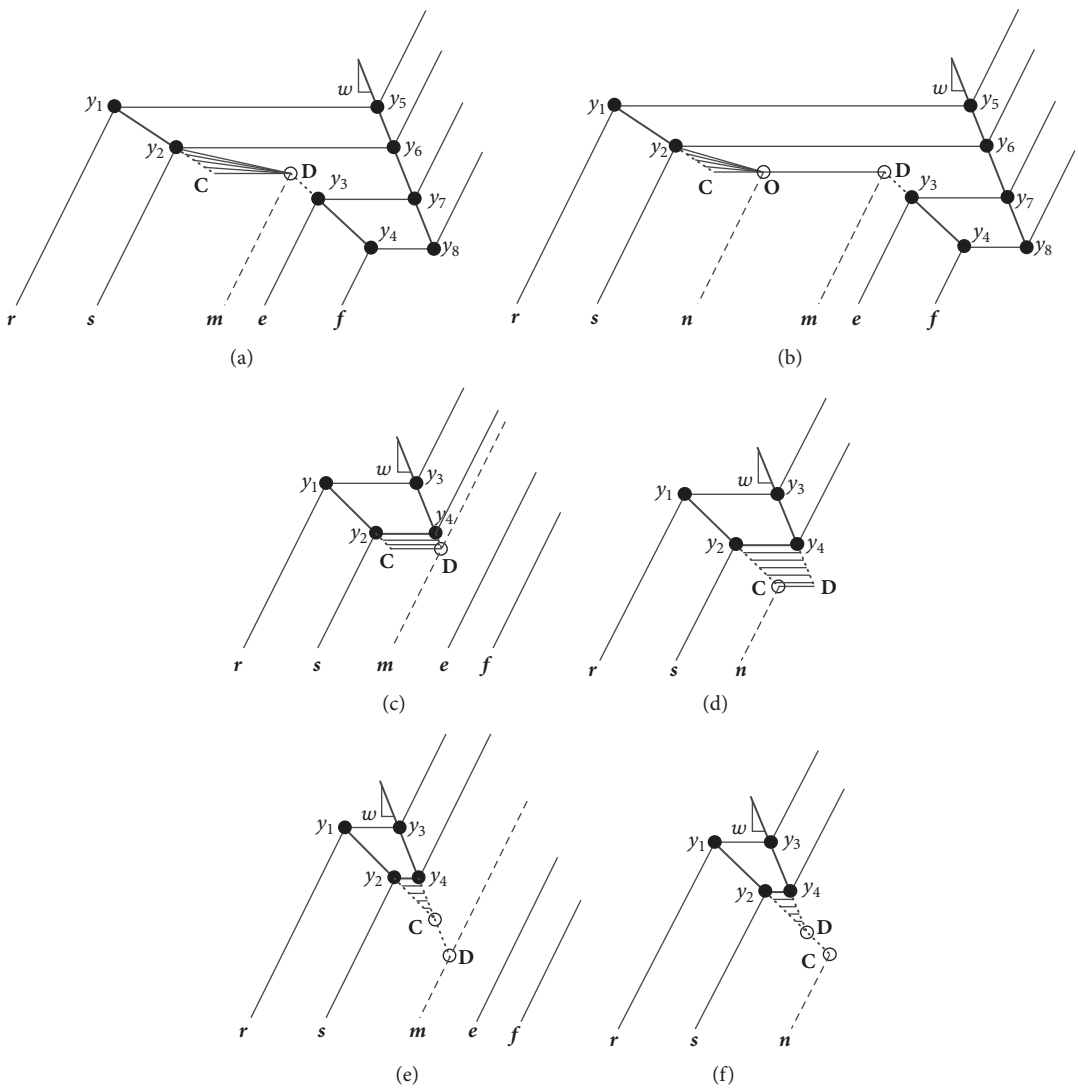

Figure 10: An illustration of handling missing data while constructing the shockwave queueing profiles using very limited mobile sensing data.

extreme case, while the real case can be any one between y_2y_4 and CD. Moreover, Figures 10(e) and 10(f) present two special but possible cases of Figures 10(c) and 10(d).

The combination of the cases in Figure 10 could very likely happen in practice. For instance, with Figures 10(a) and 10(d) in mind, Figure 11(a) illustrates the reconstruction of the shockwave profiles, under the assumption that each subflow contains only two CVs, e.g., r and s and c and d. More specifically, the shockwave forming curve $y_2\mathrm{D}y_3$ and the queue end EF can be fixed. Albeit not fully accurate, our simulation studies in Section 5 demonstrate that the inaccuracy is not essential as far as the total delay estimate is concerned (Theorem 6).

4.2.2. The Case of One Connected Vehicle in Each Subflow. At an early stage of the CV deployment, it may not be even practical to assume two CVs available in each flow from the upstream. So, it is necessary to also consider the case that only one CV is involved in some flows. Let us focus on Figure 11(b), where vehicle s and f are the only CVs within their respective flows. We again consider a virtual car n that may leave the upstream intersection at the end of the green phase that is associated with vehicle f. Then, we can fix point E with the shockwave dissolving speed w determined with y_6 and y_8. Furthermore, with the information of y_4 and the trajectory of virtual vehicle m that leaves at the start of the upstream green phase, we can determine point D. With D and y_2, we can determine point B.

Once the shockwave profile is fixed, the deterministic profile can also be plotted on the basis of Theorems 1, 2, and 4; see the illustrated correspondence between points A–E with points A′–E′ in Figure 11.

It should be emphasized that this work only requires the following information of the application site: density k_{jam} of the concerned road link, the start and end times of the signal phases at the upstream intersection and the subject intersection, and the position and speed information of CVs.

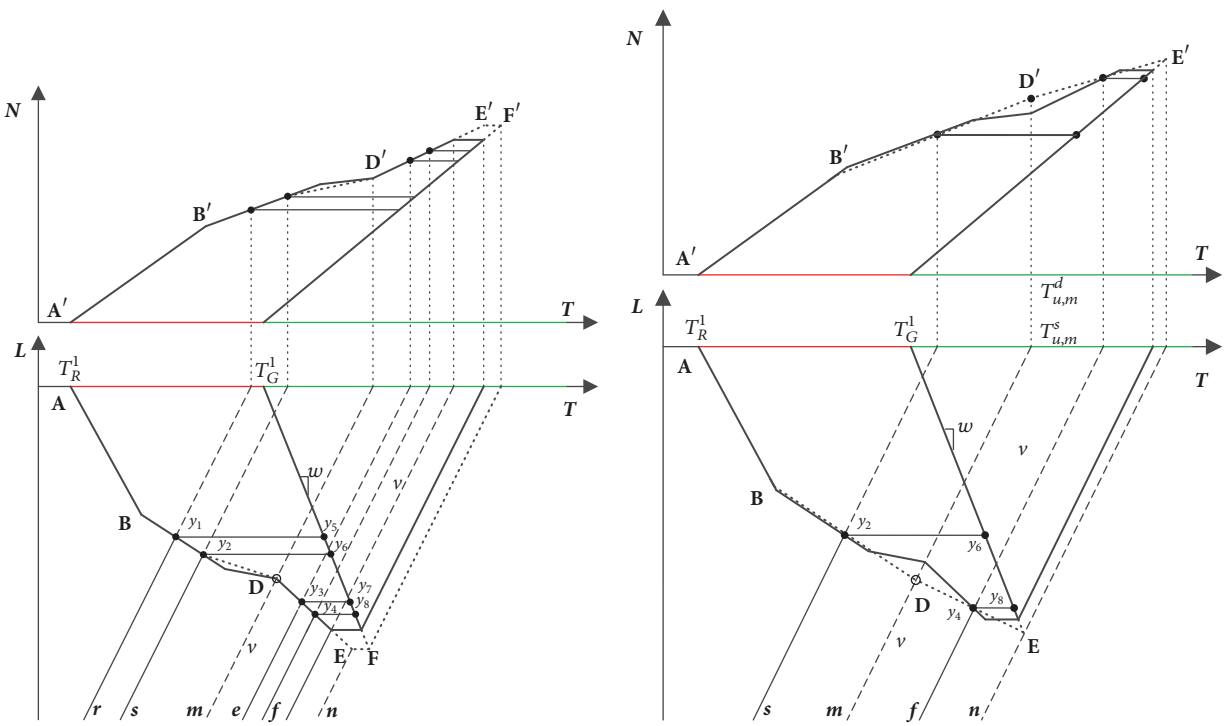

Figure 11: Further consideration for the queueing profile reconstruction.

5. Microscopic Simulation Evaluation

So far, we have discussed how to construct the shockwave and deterministic queueing profiles with very limited mobile sensing data. This section aims to evaluate the accuracy of the profile construction using the microscopic traffic simulator AIMSUN. Note that it makes little sense to do the evaluation on any performance index concerning individual cars, as the CV penetration rate is very low. Rather, we handle the evaluation on the basis of the total vertical and horizontal queue delays, which have been discussed with Theorem 6. More specifically, the ground truth is the sum of delays of all emulated individual vehicles over the simulation time horizon. The two intersections considered are 300 meters apart. The phase plan of the upstream intersection is given in Figure 12 with reference to Figure 8. The subject intersection at the downstream follows the same four-phase signal plan, with equal green and red phases of 30 s for the traffic flow from the concerned approach. The demands for the through, left-turn, and right-turn traffic at the upstream intersection (Figure 8) are 600 veh/h, 250 veh/h, and 150 veh/h. The jam density k_{jam} of the considered road link is determined with simulation to be 0.202 veh/m/lane. The simulation time horizon is 20 min. The simulation results are shown in Figure 7, but we focus on the period of the five most congested cycles from 270 s to 570 s.

By Theorem 6, we evaluate the accuracy of the profile construction based on the estimated total delay using both deterministic and shockwave profiles in comparison to the ground truth. The corresponding results are presented in

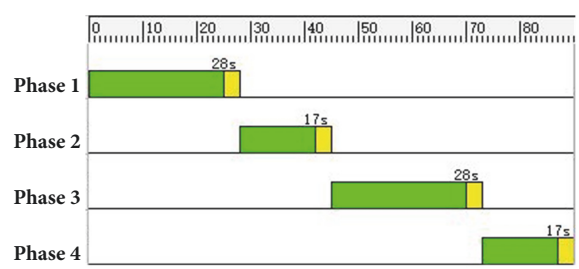

Figure 12: The phase plan for the upstream intersection.

Table 1. Clearly, the total delays determined with the two queueing profiles are quite close to the ground truth.

As shown in Figure 7(a), 10 flows are involved. Except flow ⑨, each of those flows contains more than two vehicles. We assume each flow other than ⑨ contributes at most two CVs, and the only vehicle in flow ⑨ is a CV. We have then considered 10 different cases as displayed in Table 2. In each case, the blank space means the corresponding flow has two CVs while the cross means the corresponding flow has only one CV. From top to bottom in Table 2, the number of CVs is reduced by 1 each case. Finally, in case ⑩, every flow has only one CV. The 10 flows are of different volumes. The sequence of adding the cross signs is determined as follows: the less the volume that one flow has, the higher the possibility that it has only one CV.

Focusing on the five most congested cycles in Figure 7(a), Figures 13–15 present the queueing profiles constructed for all 10 cases aforementioned. The blue curves address the cases

Table 1: Comparison of total delay between the two queueing profiles in the case of 100% penetration rate.

	Delay of 100% CVs	Ratio by the ground truth
Deterministic	2405.00	98.52%
Shockwave	2341.72	95.93%
Ground truth	2441.20	100.00%

Table 2: Ten cases.

	①	②	③	④	⑤	⑥	⑦	⑧	⑨	⑩
case 1									×	
case 2			×						×	
case 3			×						×	×
case 4			×			×			×	×
case 5	×		×			×			×	×
case 6	×		×			×	×		×	×
case 7	×		×	×		×	×		×	×
case 8	×		×	×	×	×	×		×	×
case 9	×	×	×	×	×	×	×		×	×
case 10	×	×	×	×	×	×	×	×	×	×

of 100% penetration rate, while the red curves correspond to the cases with at most two CVs in each subflow. It is noted that each horizontal pair of star signs represents a CV queueing. The corresponding penetration rate and estimation performance for each case are presented in Table 3.

Even in the extreme case ⑩, the performance is still acceptable. This indicates that the new technologies of mobile sensing have the potential of enabling even with a very low market penetration rate of connected vehicles a number of tasks that would otherwise be unpractical.

6. Conclusion

This paper addresses via analytical studies and microscopic simulations the lasting debates on the consistency between the deterministic/point/vertical queue model and the shockwave/physical/horizontal queue model, particularly with regard to oversaturated signal intersections. This paper also develops an efficient approach to the quasi-real-time reconstruction of the deterministic and shockwave queueing profiles using very limited mobile sensing data. Microscopic simulations with AIMSUN have demonstrated the efficiency of the approach as well as the analytical results obtained.

Appendix

A. The Case of a Constant Upstream Demand

For the convenience of mathematical derivation, the proof is presented in the sequence of Theorems 1, 2-(1), and 4, Corollary 5, Theorem 2-(2), Corollary 3, and Theorem 6.

Proof of Theorem 1.

(1) $\theta = 1$. Note in Figure 2 that the $N^1_{\max}$th vehicle in the deterministic profile is exactly vehicle o involved with the shockwave profile. Then, with the deterministic profile,

$$N^1_{\max} = \left(T^1_G - T^1_R\right) \cdot \frac{q_s \cdot q_u}{q_s - q_u}$$
$$T^{d,1}_E = T^1_R + \frac{N^1_{\max}}{q_u} \tag{A.1}$$

Based on the shockwave profile,

$$L^1_{\max} = \left(T^1_G - T^1_R\right) \cdot \frac{|x| \cdot |w|}{|w| - |x|}$$
$$T^1_{\max} = T^1_R + \frac{L^1_{\max}}{|x|} \tag{A.2}$$
$$T^{s,1}_E = T^1_{\max} + \frac{L^1_{\max}}{v}$$

Then, it is easy to check $T^{s,1}_E = T^{d,1}_E$.

(2) $\theta = 2$. Note that the $N^2_{\max}$th vehicle in the deterministic profile and vehicle n in the shockwave profile are the same vehicle. Then, with the deterministic profile,

$$N^1_C = \left(T^2_R - T^1_G\right) \cdot q_s \tag{A.3}$$

$$N^2_{\max} = \left(\left(T^1_G - T^1_R\right) + \left(T^2_G - T^2_R\right)\right) \cdot \frac{q_s \cdot q_u}{q_s - q_u} \tag{A.4}$$

$$T^{d,2}_E = T^1_R + \frac{N^2_{\max}}{q_u} \tag{A.5}$$

Based on the shockwave profile,

$$L^2_{\min} = \left(T^{s,1}_E - T^2_R\right) \cdot \frac{|w| \cdot v}{|w| + v} \tag{A.6}$$

$$T^2_{\min} = T^2_R + \frac{L^2_{\min}}{|w|} \tag{A.7}$$

$$L^2_{\max} = L^2_{\min} + \left(T^2_G - T^2_R\right) \cdot \frac{|x| \cdot |w|}{|w| - |x|} \tag{A.8}$$

$$T^2_{\max} = T^2_G + \frac{L^2_{\max}}{|w|} \tag{A.9}$$

$$T^{s,2}_E = T^2_{\max} + \frac{L^2_{\max}}{v} \tag{A.10}$$

Then, it is ready to see $T^{s,2}_E = T^{d,2}_E$. □

Proof of Theorem 2-(1). Consider for instance vehicle i in Figure 2. If it kept moving at its original speed after it joins the horizontal queue, it would reach the stop line at time instant $T^s_{u,i}$. By the definition of vertical queue, $T^s_{u,i}$ is exactly the time that vehicle i joins the vertical queue, which is also time $T^d_{u,i}$

Table 3: Total delay comparison for ten cases.

Case	Number of CVs	Penetration rate	Total Delay (s)		Ratio by 100% CV data	
			Shockwave	Deterministic	Shockwave	Deterministic
1	19	22.62%	2412.16	2464.28	103.01%	102.46%
2	18	21.43%	2447.29	2508.28	104.51%	104.29%
3	17	20.24%	2429.25	2491.90	103.74%	103.61%
4	16	19.05%	2394.53	2477.85	102.26%	103.03%
5	15	17.86%	2415.03	2467.55	103.13%	102.60%
6	14	16.67%	2430.02	2497.02	103.77%	103.83%
7	13	15.48%	2419.52	2483.11	103.32%	103.25%
8	12	14.29%	2413.91	2409.39	103.08%	100.18%
9	11	13.10%	2405.28	2421.46	102.71%	100.68%
10	10	11.90%	2205.30	2204.71	94.17%	91.67%

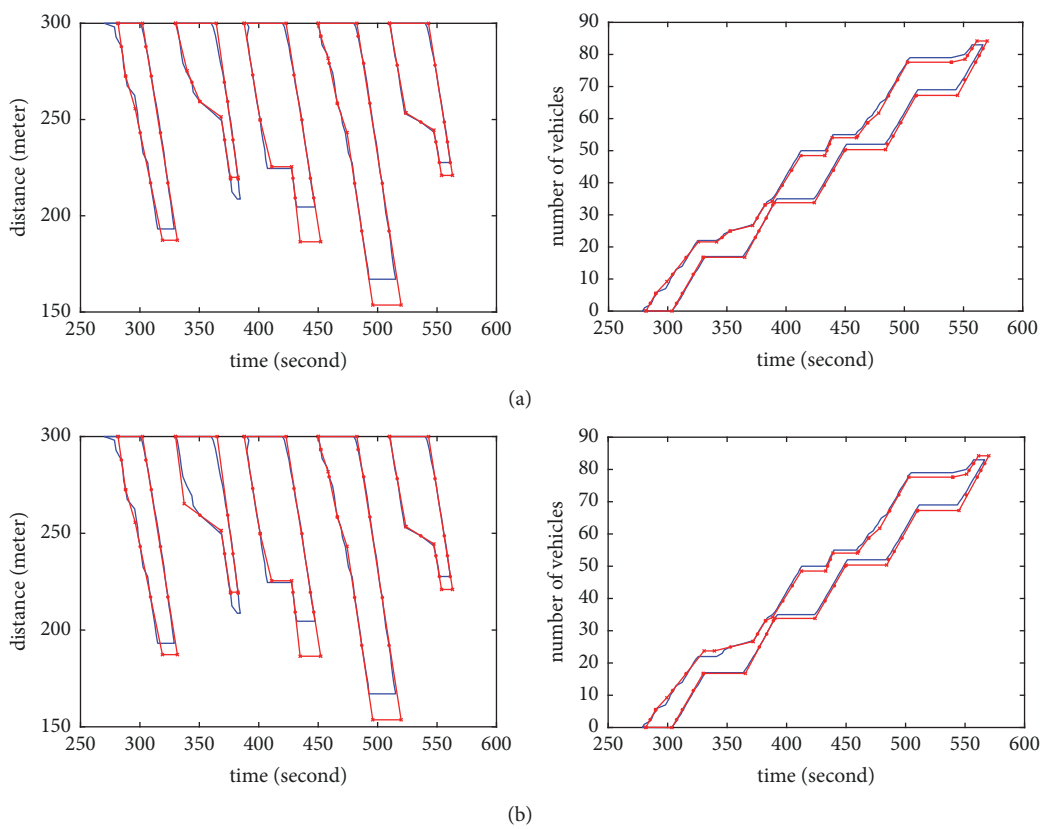

Figure 13: Reconstruction of queueing profiles for cases 1-2 in Table 2.

recorded on the arrival curve of the deterministic profile, i.e., $T^s_{u,i} = T^d_{u,i}$. Similarly, this conclusion also holds for vehicles p and m in Figure 2. In general, for any vehicle φ,

$$T^s_{u,\varphi} = T^d_{u,\varphi}. \tag{A.11}$$

□

Proof of Theorem 4. Without loss of generality, the proof is given with regard to vehicles i, p, and m in Figure 2.

Vehicle i. Based on the shockwave profile,

$$\begin{aligned} T^s_{u,i} &= T^1_R + \frac{L^1_i}{|x|} + \frac{L^1_i}{v} \\ &= T^1_R + \frac{L^1_i}{q_u} \cdot k_{\text{jam}} \end{aligned} \tag{A.12}$$

Based on the deterministic profile,

$$T^d_{u,i} = T^1_R + \frac{N_i}{q_u} \tag{A.13}$$

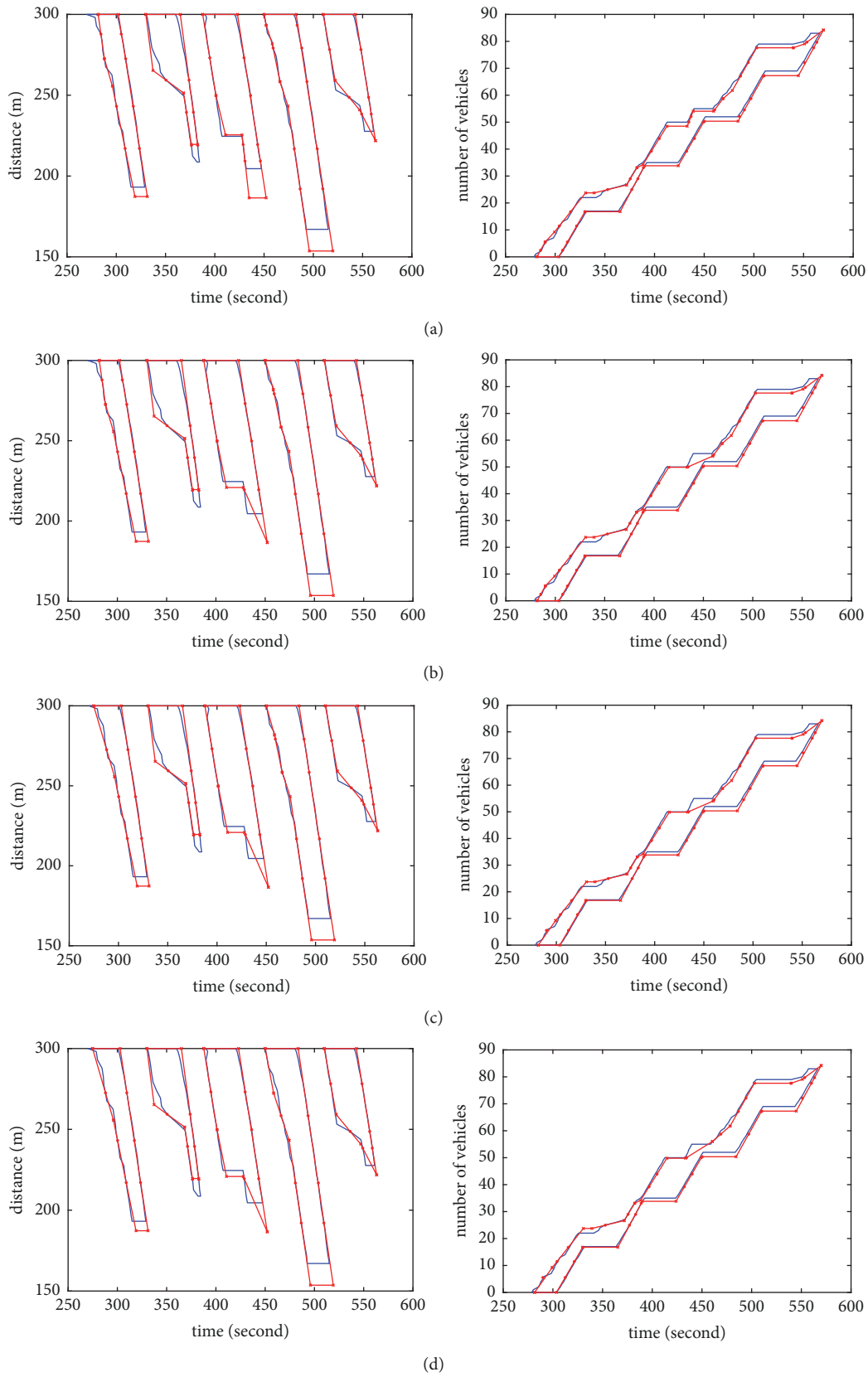

Figure 14: Reconstruction of queueing profiles for cases 3–6 in Table 2.

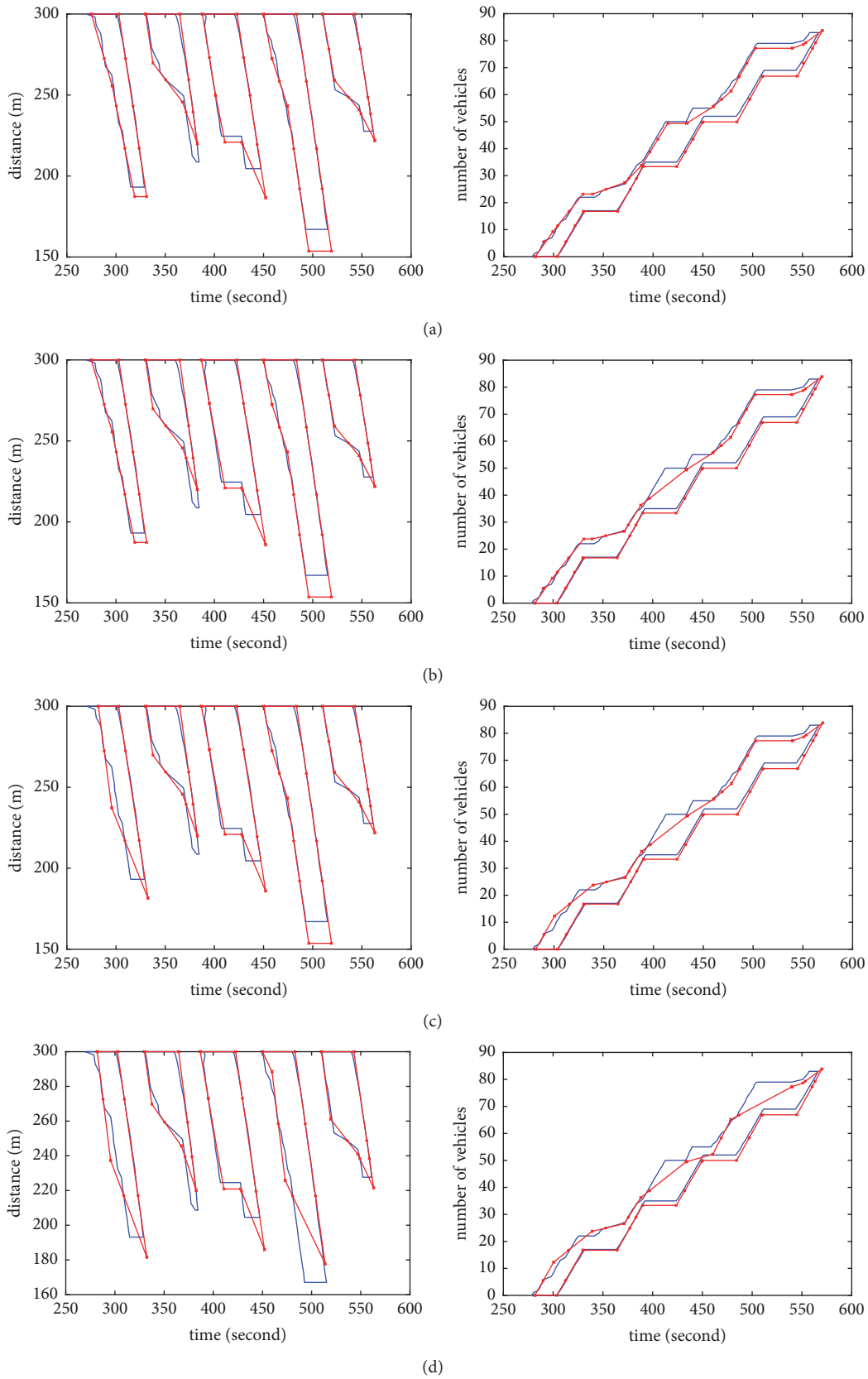

Figure 15: Reconstruction of queueing profiles for cases 7–10 in Table 2.

Thus, we have, by (A.11),

$$N_i = L_i^1 \cdot k_{\text{jam}} \tag{A.14}$$

Vehicle p. Concerning the first cycle, it can be similarly verified:

$$N_p = L_p^1 \cdot k_{\text{jam}}, \tag{A.15}$$

For the second cycle, based on the shockwave profile in Figure 2,

$$T_G^1 + \frac{L_p^1}{|w|} + \frac{L_p^1}{v} = T_R^2 + \frac{L_p^2}{|w|} + \frac{L_p^2}{v} \tag{A.16}$$

Then,

$$L_p^1 = \frac{N_C^1}{k_{\text{jam}}} + L_p^2 \tag{A.17}$$

Substituting (A.17) into (A.15) leads to

$$N_p - N_C^1 = L_p^2 \cdot k_{\text{jam}} \tag{A.18}$$

Vehicle m. Based on the shockwave profile and (A.6),

$$\begin{aligned} T_{u,m}^s &= T_R^2 + \frac{L_{\min}^2}{|w|} + \frac{L_m^2 - L_{\min}^2}{|x|} + \frac{L_m^2}{v} \\ &= T_R^1 + \frac{N_C^1}{q_u} + \frac{L_m^2 \cdot k_{\text{jam}}}{q_u} \end{aligned} \tag{A.19}$$

With the deterministic diagram,

$$T_{u,m}^d = T_R^1 + \frac{N_m}{q_u} \tag{A.20}$$

Then, by (A.11),

$$N_m - N_C^1 = L_m^2 \cdot k_{\text{jam}} \tag{A.21}$$

□

Proof of Corollary 5. For vehicle p queueing twice as illustrated in Figure 2, we can see by (A.3) and (A.17) that $L_p^2 = L_p^1 - ((T_R^2 - T_G^1) \cdot q_s)/k_{\text{jam}}$. □

Proof of Theorem 2-(2).

Vehicle i. Based on the shockwave profile in Figure 2,

$$\begin{aligned} T_{s,i}^s &= T_G^1 + \frac{L_i}{|w|} + \frac{L_i}{v} \\ &= T_G^1 + \frac{L_i}{q_s} \cdot k_{\text{jam}} \end{aligned} \tag{A.22}$$

With the deterministic profile,

$$T_{s,i}^d = T_G^1 + \frac{N_i}{q_s} \tag{A.23}$$

By (A.22), (A.23), and (A.14), we see that $T_{s,i}^d = T_{s,i}^s$ for any vehicle i.

Vehicle p. Similarly, it can be verified that $T_{s,p}^{d,1} = T_{s,p}^{s,1}$ for any vehicle p.

Based on the shockwave profile,

$$\begin{aligned} T_{s,p}^{s,2} &= T_G^2 + \frac{L_p^2}{|w|} + \frac{L_p^2}{v} \\ &= T_G^2 + \frac{L_p^2}{q_s} \cdot k_{\text{jam}} \end{aligned} \tag{A.24}$$

With the deterministic profile,

$$T_{s,p}^{d,2} = T_G^2 + \frac{N_p - N_C^1}{q_s} \tag{A.25}$$

Then, we know from (A.24), (A.25), and (A.18) that $T_{s,p}^{d,2} = T_{s,p}^{s,2}$ for any vehicle p.

Vehicle m. Based on the shockwave profile,

$$\begin{aligned} T_{s,m}^s &= T_G^2 + \frac{L_m^2}{|w|} + \frac{L_m^2}{v} \\ &= T_G^2 + \frac{L_m^2}{q_s} \cdot k_{\text{jam}} \end{aligned} \tag{A.26}$$

With the deterministic profile,

$$T_{s,p}^d = T_G^2 + \frac{N_m - N_C^1}{q_s} \tag{A.27}$$

Via (A.26), (A.27), and (A.21), we have $T_{s,m}^d = T_{s,m}^s$ for any vehicle m. □

Proof of Corollary 3. Based on the definitions of queueing delay, $d_\varphi^d = T_{s,\varphi}^d - T_{u,\varphi}^d$, $d_\varphi^s = T_{s,\varphi}^s - T_{u,\varphi}^s$ (if φ is involved with one cycle) or $d_\varphi^s = T_{s,\varphi}^{s,2} - T_{u,\varphi}^s$ (if φ is involved with two cycles). Then, it is straightforward with Theorem 2 that Corollary 3 holds. □

Proof of Theorem 6. As illustrated with Figure 16, there exists one-to-one correspondence between the deterministic and shockwave profiles in terms of vehicle delays. In what follows, we use subscript "H" to represent the horizontal queue and subscript "V" to represent the vertical queue.

Case ①. With the deterministic profile in Figure 16,

$$S_{V,1} = \frac{1}{2} \cdot \left(T_G^1 - T_R^1\right) \cdot N_{\max}^1 \tag{A.28}$$

Based on the shockwave profile,

$$S_{H,1} = \frac{1}{2} \cdot \left(T_G^1 - T_R^1\right) \cdot L_{\max}^1 \tag{A.29}$$

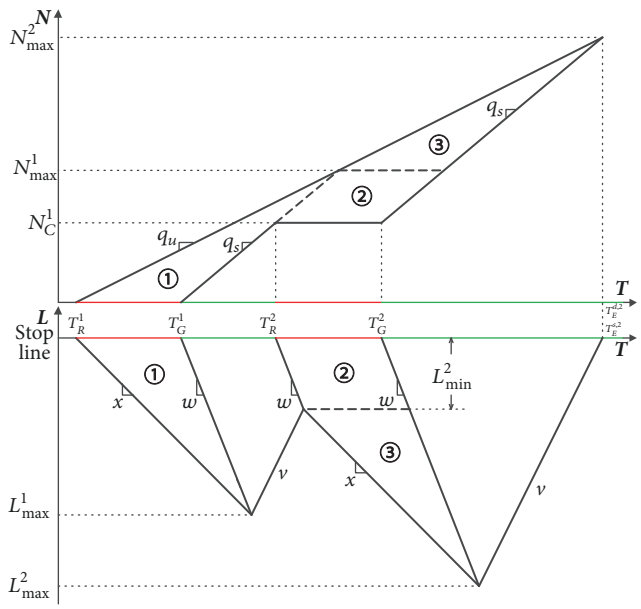

Figure 16: Deterministic and shockwave profiles with their total delay connection.

Based on Theorem 4, we have $N^1_{\max} = L^1_{\max} \cdot k_{\text{jam}}$ for vehicle o (in Figure 2); then $S_{V,1} = S_{H,1} \cdot k_{\text{jam}}$.

Case ②

$$\begin{aligned} S_{V,2} &= \left(T^2_G - T^2_R\right) \cdot \left(N^1_{\max} - N^1_C\right) \\ S_{H,2} &= \left(T^2_G - T^2_R\right) \cdot L^2_{\min} \end{aligned} \tag{A.30}$$

Again, based on Theorem 4 and Figure 2, $N^1_{\max} - N^1_C = L^2_{\min} \cdot k_{\text{jam}}$ for vehicle o (in Figure 2); we have $S_{V,2} = S_{H,2} \cdot k_{\text{jam}}$.

Case ③

$$\begin{aligned} S_{V,3} &= \left(T^2_G - T^2_R\right) \cdot \left(N^2_{\max} - N^1_{\max}\right) \\ S_{H,3} &= \left(T^2_G - T^2_R\right) \cdot \left(L^2_{\max} - L^2_{\min}\right) \end{aligned} \tag{A.31}$$

Based on Theorem 4, $N^1_{\max} - N^1_C = L^2_{\min} \cdot k_{\text{jam}}$ and $N^2_{\max} - N^1_C = L^2_{\max} \cdot k_{\text{jam}}$; then we have $S_{V,3} = S_{H,3} \cdot k_{\text{jam}}$.

Since $S_V = S_{V,1} + S_{V,2} + S_{V,3}$ and $S_H = S_{H,1} + S_{H,2} + S_{H,3}$, $S_V = S_H \cdot k_{\text{jam}}$. □

B. The Case of a Varying Upstream Demand

Theorems 1, 2, 4, and 6 and Corollaries 3 and 5 still hold in this case. The corresponding proof is briefly presented with reference to Figure 6.

Proof of Theorem 1. Regardless of traffic demands, the departure curve in either profile is a straight line. With this in mind, the total number of vehicles served during the two cycles (passing the stop line) in the shockwave profile of Figure 6 can be derived as $N_H = ((T^2_R - T^1_G) + (T^{s,2}_E - T^2_G)) \cdot q_s$, under the assumption that vehicle queues are discharged during the green phase at the full capacity q_s of the intersection. This number can also be checked with the deterministic profile, and $N_V = ((T^2_R - T^1_G) + (T^{d,2}_E - T^2_G)) \cdot q_s$. Whichever of the models is used, we must have $N_V = N_H$. Thus, it can be easily verified that $T^{s,2}_E = T^{d,2}_E$. Similarly, we also have $T^{s,1}_E = T^{d,1}_E$. □

As shown in Figure 6, vehicles that join the horizontal queue over section AB can be regarded as those of a constant upstream demand. Thus, Theorems 2 and 4 apply to all these vehicles, including vehicle i. Then, the question is if Theorems 2 and 4 also apply to all vehicles that arrive over section BC provided that Theorems 2 and 4 apply to vehicle i at point B. If it is true, Theorems 2 and 4 can be proved with mathematical induction for the deterministic and shockwave profiles in Figure 6, as long as the arrival curve in either profile is piecewise linear.

Without loss of generality, the proof is given below with respect to vehicles r and p in Figure 6. The proof process is essentially the same as that in the case of a constant demand. First, for vehicle i, we have, by Theorems 2 and 4,

$$T^d_{u,i} = T^s_{u,i} \tag{B.1}$$

$$N_i = L^1_i \cdot k_{\text{jam}} \tag{B.2}$$

Proof of Theorem 2-(1). Irrespective of the demand condition, this holds following the definitions of vertical and horizontal queues. □

Proof of Theorem 4. Without loss of generality, it suffices to check the cases of vehicles r and p.

Vehicle r. Based on the deterministic profile in Figure 6,

$$T^d_{u,r} = T^d_{u,i} + \frac{N_r - N_i}{q_{\text{BC}}}, \tag{B.3}$$

where q_{BC} denotes the upstream arrival flow for section BC.

Based on the shockwave profile,

$$\begin{aligned} T^s_{u,r} &= T_{a,i} + \frac{L^1_r - L^1_i}{|x_{\text{BC}}|} \\ &\quad + \frac{L^1_r}{v} \left(T_{a,i} \text{ is defined in Figure 2}\right) \\ &= T_{a,i} + \frac{L^1_i}{v} + \frac{L^1_r - L^1_i}{|x_{\text{BC}}|} + \frac{L^1_r - L^1_i}{v} \\ &= T^s_{u,i} + \frac{L^1_r - L^1_i}{q_{\text{BC}}/\left(k_{\text{jam}} - k_2\right)} + \frac{L^1_r - L^1_i}{q_{\text{BC}}/k_2} \\ &= T^s_{u,i} + \frac{L^1_r - L^1_i}{q_{\text{BC}}} \cdot k_{\text{jam}} \end{aligned} \tag{B.4}$$

Then, we have by (B.1)

$$N_r - N_i = \left(L^1_i - L^1_r\right) \cdot k_{\text{jam}} \tag{B.5}$$

Also, with (B.2) for vehicle i, it is straightforward to get

$$N_r = L_r^1 \cdot k_{\text{jam}} \tag{B.6}$$

Vehicle p. For the first cycle, like (B.6), it can be similarly verified that

$$N_p = L_p^1 \cdot k_{\text{jam}} \tag{B.7}$$

For the second cycle, based on the shockwave profile in Figure 6,

$$T_G^1 + \frac{L_p^1}{|w|} + \frac{L_p^1}{v} = T_R^2 + \frac{L_p^2}{|w|} + \frac{L_p^2}{v} \tag{B.8}$$

Then, by (A.3)

$$L_p^1 = \frac{N_C^1}{k_{\text{jam}}} + L_p^2 \tag{B.9}$$

Substituting (B.9) into (B.7) leads to

$$N_p - N_C^1 = L_p^2 \cdot k_{\text{jam}} \tag{B.10}$$

Thus, Theorem 4 holds for any vehicle p. □

Proof of Corollary 5. For vehicle p in Figure 6, via (A.3) and (B.9), $L_p^2 = L_p^1 - ((T_R^2 - T_G^1) \cdot q_s)/k_{\text{jam}}$. □

Proof of Theorem 2-(2). Again, it suffices to check vehicles r and p.

Vehicle r. With the deterministic profile,

$$T_{s,r}^d = T_G^1 + \frac{N_r}{q_s} \tag{B.11}$$

And by the shockwave profile,

$$\begin{aligned} T_{s,r}^s &= T_G^1 + \frac{L_r^1}{|w|} + \frac{L_r^1}{v} \\ &= T_G^1 + \frac{L_r^1}{q_s} \cdot k_{\text{jam}} \end{aligned} \tag{B.12}$$

By (B.11) and (B.12) as well as (B.6), we see that $T_{s,r}^d = T_{s,r}^s$ for any vehicle r.

Vehicle p. Similarly, it can be verified that $T_{s,p}^{d,1} = T_{s,p}^{s,1}$ for any vehicle p.

Based on the shockwave profile in Figure 6,

$$\begin{aligned} T_{s,p}^{s,2} &= T_G^2 + \frac{L_p^2}{|w|} + \frac{L_p^2}{v} \\ &= T_G^2 + \frac{L_p^2}{q_s} \cdot k_{\text{jam}} \end{aligned} \tag{B.13}$$

Based on the deterministic profile in Figure 6,

$$T_{s,p}^{d,2} = T_G^2 + \frac{N_p - N_C^1}{q_s} \tag{B.14}$$

Then, we know from (B.10), (B.13), and (B.14) that $T_{s,p}^{d,2} = T_{s,p}^{s,2}$ for any vehicle p. □

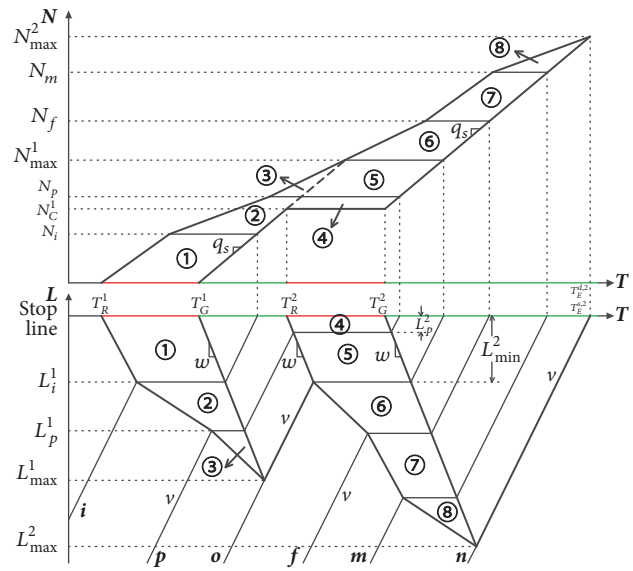

Figure 17: Deterministic and shockwave queueing profiles with their total delay correlation under a varying traffic demand.

As discussed above, Theorems 2 and 4 hold for any vehicle over BC provided that the theorems hold for vehicle i at point B. Similarly, it can also be proved that Theorems 2 and 4 hold for any vehicle over CD provided that the theorems hold for vehicle p at point C. As such, it can be proved that Theorems 2 and 4 hold for the whole shockwave and deterministic queueing profiles as long as the upstream demand is such that both queue forming curves are piecewise linear.

Proof of Corollary 3. The proof is straightforward. □

Proof of Theorem 6. As displayed with Figure 17, there exists one-to-one correspondence between the deterministic and shockwave profiles in terms of delay. The proof is similar to that for Theorem 6 in Appendix A. □

Conflicts of Interest

The authors declare that they have no conflicts of interest.

Authors' Contributions

Yongyang Liu and Jingqiu Guo contributed equally to this work and share the first authorship.

Acknowledgments

The research reported in this paper was supported in part by the Zhejiang Qianren Program (4013-2018) and the National Natural Science Foundation of China (51478428; 71771200).

References

[1] K. Moskowitz and L. Newman, "Notes on freeway capacity," Highway Research Board 27, 1963.

[2] D. C. Gazis and R. B. Potts, "The over-saturated intersection," in *Proceedings of the 2nd International Symposium on the Theory of Road Traffic Flow*, pp. 221–237, 1965.

[3] C. F. Daganzo, *Fundamentals of Transportation and Traffic Operations*, Pergamon, Oxford, UK, 1997.

[4] M. J. Lighthill and G. B. Whitham, "On kinematic waves. II. A theory of traffic flow on long crowded roads," *Proceedings of the Royal Society A Mathematical, Physical and Engineering Sciences*, vol. 229, no. 1178, pp. 317–345, 1955.

[5] P. I. Richards, "Shock waves on the highway," *Operations Research*, vol. 4, no. 1, pp. 42–51, 1956.

[6] W. R. McShane and R. P. Roess, *Traffic Engineering*, Prentice Hall, Inc., Upper Saddle River, NJ, USA, 2nd edition, 1998.

[7] Y. Makigami, G. F. Newell, and R. Rothery, "Three-dimensional representation of traffic flow," *Transportation Science*, vol. 5, no. 3, pp. 302–313, 1971.

[8] S. C. Wirasinghe, "Determination of traffic delays from shock-wave analysis," *Transportation Research*, vol. 12, no. 5, pp. 343–348, 1978.

[9] P. G. Michalopoulos and V. B. Pisharody, "Derivation of delays based on improved macroscopic traffic models," *Transportation Research Part B: Methodological*, vol. 15, no. 5, pp. 299–317, 1981.

[10] C. F. Daganzo, "Derivation of delays based on input-output analysis," *Transportation Research Part A: General*, vol. 17, no. 5, pp. 341-342, 1983.

[11] H.-C. Chin, "A reexamination of the analysis of freeway bottlenecks," *ITE Journal (Institute of Transportation Engineers)*, vol. 66, no. 1, pp. 30–35, 1996.

[12] D. H. Nam and D. R. Drew, "Analyzing freeway traffic under congestion: traffic dynamics approach," *Journal of Transportation Engineering*, vol. 124, no. 3, pp. 208–212, 1998.

[13] T. W. Lawson, D. J. Lovell, and C. F. Daganzo, "Using input-output diagram to determine spatial and temporal extents of a queue upstream of a bottleneck," *Transportation Research Record: Journal of the Transportation Research Board*, no. 1572, pp. 140–147, 1997.

[14] A. L. Erera, T. W. Lawson, and C. F. Daganzo, "Simple, generalized method for analysis of traffic queue upstream of a bottleneck," *Transportation Research Record: Journal of the Transportation Research Board*, no. 1646, pp. 132–140, 1998.

[15] D. J. Lovell and J. R. Windover, "Analyzing freeway traffic under congestion: Traffic dynamics approach," *Journal of Transportation Engineering*, vol. 125, no. 4, pp. 373–375, 1999.

[16] H. Rakha and W. Zhang, "Consistency of shock-wave and queuing theory procedures for analysis of roadway bottlenecks," in *Proceedings of the 84th Annual Meeting of the Transportation Research Board*, Washington, DC, USA, 2005.

[17] P. Yi, Z.-Z. Tian, and Q. Zhao, "Consistency of input-output model and shockwave analysis in queue and delay estimations," *Journal of Transportation Systems Engineering and Information Technology*, vol. 8, no. 6, pp. 146–152, 2008.

[18] H. X. Liu, X. W. Wu, Ma., and H. Hu, "Real-time queue length estimation for congested signalized intersections," *Transportation Research Part C: Emerging Technologies*, vol. 17, no. 4, pp. 412–427, 2009.

[19] A. Skabardonis and N. Geroliminis, "Real-time monitoring and control on signalized arterials," *Journal of Intelligent Transportation Systems: Technology, Planning, and Operations*, vol. 12, no. 2, pp. 64–74, 2008.

[20] A. Sharma, D. M. Bullock, and J. A. Bonneson, "Input-output and hybrid techniques for real-time prediction of delays and maximum queue length at a signalized intersection," *Journal of Transportation Research Record*, no. 2035, pp. 88–96, 2007.

[21] F. Dion, H. Rakha, and Y. Kang, "Comparison of delay estimates at under-saturated and over-saturated pre-timed signalized intersections," *Transportation Research Part B: Methodological*, vol. 38, no. 2, pp. 99–122, 2004.

[22] Z. Sun and J. Ban, "Vehicle trajectory reconstruction for signalized intersections using mobile traffic sensors," *Transportation Research Part C: Emerging Technologies*, vol. 36, pp. 268–283, 2013.

[23] X.-Y. Lu and A. Skabardonis, "Freeway traffic shockwave analysis: exploring ngsim trajectory data," in *Proceedings of the 86th Annual Meeting of the Transportation Research Board*, Washington, DC, USA, 2007.

[24] P. Izadpanah, B. Hellinga, and L. Fu, "Automatic traffic shockwave identification using vehicles' trajectories," in *Proceedings of the 88th Annual Meeting of the Transportation Research Board*, 2009.

[25] Y. Cheng, X. Qin, J. Jin, and B. Ran, "An exploratory shockwave approach for signalized intersection performance measurements using probe trajectories," in *Proceedings of the Transportation Research Board 89th Annual Meeting*, 2010.

[26] K. Yang and M. Menendez, "A convex model for queue length estimation in a connected vehicle environment," in *Proceedings of the 96th Annual Meeting of Transportation Research Board*, 2017.

[27] X. Ban, R. Herring, P. Hao, and A. M. Bayen, "Delay pattern estimation for signalized intersections using sampled travel times," *Transportation Research Record: Journal of the Transportation Research Board*, vol. 2130, pp. 109–119, 2009.

[28] X. J. Ban, P. Hao, and Z. Sun, "Real time queue length estimation for signalized intersections using travel times from mobile sensors," *Transportation Research Part C: Emerging Technologies*, vol. 19, no. 6, pp. 1133–1156, 2011.

[29] P. Hao and X. Ban, "Long queue estimation for signalized intersections using mobile data," *Transportation Research Part B: Methodological*, vol. 82, pp. 54–73, 2015.